

Dynamic Fracture Properties of Titanium Alloys

D.D. Anderson · A.J. Rosakis

Received: 25 August 2005 / Accepted: 31 October 2005 / Published online: 7 March 2006
© Society for Experimental Mechanics 2006

Abstract Fatigue precracked specimens of three titanium alloys (6Al-4V, ELI, and Timetal 5111) were dynamically loaded in a drop weight tower system while the dynamic fracture toughness was inferred using Coherent Gradient Sensing, crack opening displacement, or strain gage methods. A comparison of the initiation toughness of the three materials as a function of loading rate and specimen thickness is made.

Keywords Dynamic fracture properties · Titanium · Experimental measurement techniques

Introduction

With ductile/advanced materials being used in increasingly demanding applications, a more thorough understanding of their fracture behavior is essential. For some materials (such as aluminum) the critical dynamic stress intensity factor K_{IC}^d for some loading rates can be *less* than the quasistatic stress intensity factor K_{IC} generally used to specify a material's fracture toughness. Consequently, for reliable and efficient use a material's fracture behavior over the entire

envelope of anticipated service conditions should be understood.

This paper describes the use of three measurement techniques to determine the dynamic fracture properties of three titanium alloys. The techniques are: Coherent Gradient Sensing (CGS), Crack Opening Displacement (COD), and the use of strain gages. While these techniques are briefly described below, a more detailed description and comparison of the techniques is available in Anderson and Rosakis [1]. Some observations are made regarding rate and thickness effects on fracture toughness.

Previous work on the experimental determination of material dynamic fracture properties of engineering materials is very limited. Most dynamic failure studies have utilized materials with ideal properties, typically polymers. For example, dynamically loaded Homalite-100 fracture properties were studied using the optical method of caustics by Ravi-Chandar and Knauss [2]. Dynamic crack initiation in PMMA was studied by Rittel and Maigre [3–5] using a novel hybrid analytical/experimental procedure. Transient crack growth in PMMA was examined using CGS by Freund and Rosakis [6]. Ceramic material was tested by Suresh et al. [7]. Prior work on engineering materials is limited to simple observations. For example, critical crack opening displacements for explosively loaded 1020 hot-rolled steel were obtained by Wilson, Hawley and Duffy [8]. Dynamic crack growth research of polymers using dynamic photoelasticity is described by Dally [9]. Two of the first studies of dynamic crack growth on metals were conducted by Rosakis, Duffy and Freund [10] and Zehnder and Rosakis [11] who examined highly dynamic crack growth in thick plates of AISI 4340 steel using the optical method of caustics

D.D. Anderson (✉)
General Electric Global Research Center,
One Research Circle, Niskayuna, NY 12309, USA
e-mail: Anderson@research.ge.com

A.J. Rosakis (SEM member)
Graduate Aeronautical Laboratories,
California Institute of Technology,
Pasadena, CA 91125, USA
e-mail: Rosakis@aero.caltech.edu

in reflection in conjunction with high speed photography. The dynamic initiation and propagation behavior in thin aluminum sheets was studied by Owen et al. [12]. Small specimens were loaded using a split Hopkinson bar and the stress intensity factor K_I^d was calculated using boundary measurements by assuming quasi-equilibrium. This assumption was validated by dynamic COD measurements from the thinnest sheets.

Basis for Determination of a Fracture Toughness Parameter

The origin of the stress intensity factor used to describe the magnitude of crack tip stresses dates back to 1957 due to work by Irwin [13] and Westergaard [17] with asymptotic linear elastic crack tip solutions. With this parameter, a material's fracture toughness can be established by measuring the stress intensity factor at incipient crack initiation. Standards for determining and validating a material's critical stress intensity factor for initiating a quasistatically loaded stationary crack (ASTM E399 [14]) have made fracture toughness determination routine for many structural materials. However, as with other mechanical properties, fracture toughness is generally rate dependent (Freund, Duffy and Rosakis [15], Rittel and Rosakis [16]) and the use of quasistatic values may be nonconservative.

Linear elastic fracture mechanics (LEFM) serves as a simple but sufficient analytical framework for studying fracture behavior engineering materials so long as ductility is not too great. For each LEFM crack mode, stress-fields satisfying the boundary condition of having traction-free crack faces are asymptotic with unknown coefficients reflecting unspecified far-field boundary conditions (Westergaard [17], Irwin [13], Sneddon [18], and Williams [19]) are of the form:

$$\sigma_{ij} = \left(\frac{K}{\sqrt{2\pi r}} \right) f_{ij}(\theta) + \sum_{m=0}^{\infty} A_m r^{m/2} g_{ij}^m(\theta) \quad (1)$$

where σ_{ij} are Cartesian components of the stress tensor, r and θ are spatial coordinates with respect to the usual crack tip coordinate system, f_{ij} and g_{ij}^m are functions of θ , and K and A_m are the coefficients of the singular and higher order terms respectively. f_{ij} and g_{ij}^m are known universal functions of angle θ for all cracks propagating at speeds much slower than the material's shear wave speed (Freund and Clifton [20]), including stationary cracks. References for dynamic studies

include Yoffe [21], Broberg [22], Atkinson and Eshelby [23], Achenbach [24–26], Kostrov and Nikitin [27], Freund [28–30], and Willis [31]. A single excellent source regarding dynamic fracture is Freund [32].

For each mode the leading asymptotic term is singular and thus dominates near the crack tip. Because of this dominance, the leading term's coefficient K can serve as a single parameter description of the stress state at the crack tip, i.e., the stress intensity factor. The critical value of K at incipient failure is the material's fracture toughness and is denoted K_{IC}^d for mode I (opening mode) dynamic conditions. The superscript d is omitted to signify quasistatic fracture toughness.

A stress singularity at the crack tip as modeled by LEFM cannot realistically exist in materials with finite strength. Instead the highly stressed material yields and plastically deforms. To first order the time dependent size of the plastic zone for mode I is:

$$r_p = \frac{1}{2\pi} \left(\frac{K_I^d}{\sigma_{YS}} \right)^2 \quad (2)$$

where σ_{YS} is the material yield stress. At crack initiation the critical characteristic plastic zone size, r_{pc} is determined by setting $K_I^d = K_{IC}^d$. The actual shape of the plastic zone depends on crack tip triaxiality. Because σ_{YS} is generally strain-rate dependent, r_{pc} is also dependent on crack tip loading rate and propagation speed, with the later effect dominant for growing cracks. If K_{IC}^d is also found to be rate dependant, this will also influence the critical value (r_{pc}) of r_p at crack initiation. Equation (2) defines a useful material/rate-dependent length scale for crack tip mechanics.

In situations in which a crack tip stress field is well modeled by LEFM, the plastic zone is always small enough to be completely surrounded by an annulus in which stresses are well described by the K -field. The outer extent of the K -field dominated annulus is due to the increasing relative contributions of higher order asymptotic stress field terms. This concept that LEFM can still describe crack tip fields in such cases despite crack tip yielding is called small scale yielding (S.S.Y.) (Freund and Rosakis [6]). Ignoring material yielding effects, the extent of K -field dominance is linear with the dominant structure size. Thus the applicability of S.S.Y. depends on material *and* on geometry.

The value of K_{IC}^d has dependence on specimen thickness (h/r_{pc}) and as thickness increases it asymptotically approaches a conservative limit called the plane strain fracture toughness K_{IC}^d (Irwin [33], Kanninen and Popelar [34]). This asymptotic behavior

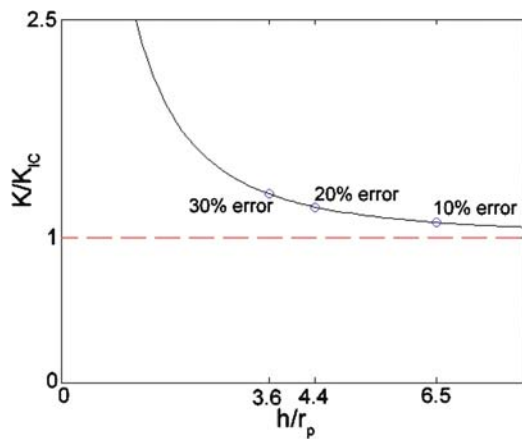


Fig. 1. Normalized initiation toughness versus specimen thickness for aluminum

is due to the effects of thickness on crack tip stress triaxiality over the crack front. The critical value K_{IC}^d is geometry independent though not independent of loading rate. A specimen may be thick enough to produce a measure of plane strain fracture toughness at a higher loading rate but not at a lower one.

By way of example, Irwin [35] empirically obtained a relationship between quasistatic fracture toughness and thickness for 7075-T6 and 2024-T4 aluminum:

$$\frac{K_{IC}^d}{K_{IC}} = \left[1 + 5.6\pi^2 \left(\frac{r_p}{h} \right)^2 \right]^{1/2} \quad (3)$$

This relationship is plotted in Fig. 1. The horizontal dashed line is the asymptotic limit of toughness as thickness increases (K_{IC}). The circle with adjacent text indicate the error in assuming $K_{IC} = K_{IC}^d$ for various values of h/r_p . While other materials exhibit the same qualitative behavior, quantitative results vary and must be obtained experimentally (Jones and Brown [36]).

Ideally plane strain values are obtained by testing thick specimens compared to plastic zone size. Plane strain values can be obtained from thinner specimens by modifying geometry to create plane strain conditions, typically by machining side-grooves. Side-grooves are “V” shaped notches cut in the sides of a specimen centered on the crack and extending the length of the specimen (Fig. 2). Side-grooves increase the triaxiality at the crack tip by reducing the amount of Poisson contraction about the tip, subjecting the crack tip to more uniformly plane strain like conditions as if the specimen were thicker.

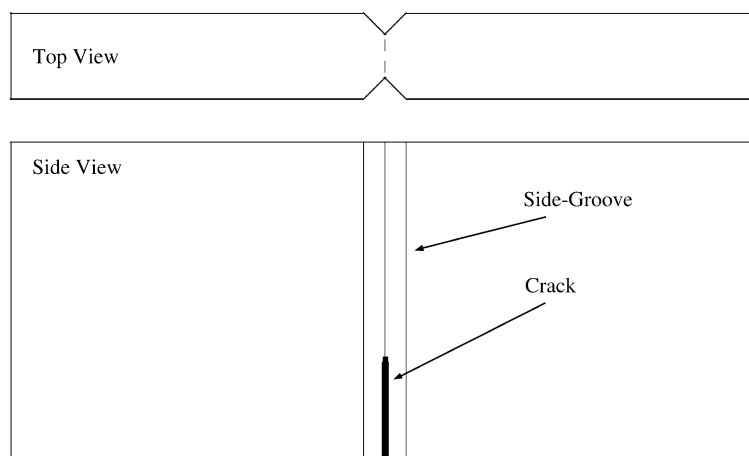
Experimental Techniques

Three measurement techniques were used to infer the dynamic fracture response of three titanium alloys. The techniques are: Coherent Gradient Sensing (CGS), Crack Opening Displacement (COD), and the use of strain gages. While a brief summary follows, a more detailed description of each technique, sources and magnitudes of error, and an experimental comparison of their measurement results on dynamically fractured titanium is available in Anderson and Rosakis [1].

Coherent Gradient Sensing

CGS is a full-field optical interferometric method which can measure surface slopes for reflective specimens and geometric and stress induced optical path gradients for transparent specimens (Tippur et al. [37, 38], Rosakis [39]). CGS produces fringes which can be related to gradients of $\hat{\sigma}_{11} + \hat{\sigma}_{22}$ for flat plates deforming under plane stress conditions. This information can then be compared to predictions by fracture

Fig. 2. Schematic of side-grooves



models to extract fracture/field parameters. Usually fringe patterns of crack tip singularities are analyzed within the context of LEFM. CGS has similarities to the optical method of caustics (Theocaris [40], Kalthoff [41], Rosakis [39]) but provides full-field measurement. Its sensitivity to *gradients of displacements* makes it ideal for measuring singular fields such as those about a crack tip. CGS is insensitive to rigid body motions and vibrations and is well suited for high speed photography, making it an ideal measurement technique for dynamic fracture studies.

As a full-field measurement technique, CGS supplies the most detailed crack information regarding the near-tip mechanical field of the three dynamic stress intensity factor measurement techniques considered in this paper. With sufficiently sophisticated data analysis, this technique can be used to provide stress intensity factor measurements for any combination of mode I and mode II loading, as well as the coefficients of the higher order terms of the crack tip asymptotic solution used. Given higher order term coefficients, the size of the K dominated field can be examined to determine K -dominance assumption validity. Crack tip position can also be determined from CGS interferograms and used to establish initiation time and calculate crack speed. By analyzing many well timed images from a single test, CGS can measure loading rate, mixed mode initiation toughness, propagation toughness, and crack speed.

CGS cannot be used on side-grooved specimens as no simple relationship exists between CGS fringe patterns and the crack tip stress field for this geometry.

Strain Gage Measurement

As shown by Dally and his coworkers [42], strain gages can be used to measure in-plane surface strains in the vicinity of cracks which can then be related to analytic asymptotic stress fields to determine stress intensity factors. This method can be employed for quasistatic or dynamic loading for both initiating and propagating cracks as material behavior allows. The primary advantages of strain gages are low cost and simplicity of analysis with essentially no special specimen preparation required. Strain gages can be used simultaneously with other measurement techniques for redundancy. Like CGS, the strain gage technique cannot be used on specimens with side grooves.

Crack Opening Displacement

Crack Opening Displacement technique involves measuring opening displacements between the crack faces

behind a single crack tip and using elastic plastic fracture mechanics (EPFM) to relate the opening displacements to the stress intensity factor.

Despite the inherent difficulty in accurately measuring crack opening and determining initiation, it can be employed on side-grooved specimens, making it invaluable for testing more ductile materials (still falling within SSY).

The relationship between crack opening displacement and stress intensity factor used for this work is from Shih [43]. This relationship is obtained using the HRR crack tip solution [44, 45] for power law hardening materials. The crack opening $\delta(r, t, n)$ is given by

$$\delta(r, t, n) = \alpha \epsilon_0 \left(\frac{J(t)}{\alpha \sigma_0 \epsilon_0 I_n} \right)^{n/n+1} r^{1/n+1} [2\tilde{u}_2(\pi, n)] \quad (4)$$

where I_n is an integration constant and J is the value of the J -integral. For a linear elastic material $J = K_I^2/E$. Other studies utilizing EPFM to determine fracture toughness include Costin and Duffy [46], Nakamura et al. [47], and Owen [12].

Materials

Three titanium alloys are tested to determine quasi-static and dynamic crack initiation toughness. The three alloys are a commercial grade 6Al-4V Titanium alloy, 6Al-4V Ti ELI, and Timetal 5111 (ASTM Grade 32). Chemical composition of the materials tested is given in Table 1 and nominal mechanical properties can be found in Table 2.

Table 1 Chemical composition of titanium alloys tested

Constituent	6Al-4V Ti	6Al-4V Ti ELI	Timetal 5111
Aluminum	6.225	5.80	4.5–5.5
Vanadium	3.875	3.96	0.6–1.4
Tin	–	–	0.6–1.4
Zirconium	–	–	0.6–1.4
Molybdenum	–	–	0.6–1.4
Nitrogen	0.013	0.015	0–0.03
Oxygen	0.19	0.073	0–0.11
Carbon	0.018	–	0–0.08
Hydrogen	0.0081	–	0–0.015
Iron	0.16	0.034	0–0.25
Yttrium	0.001	<59 ppm	–
Silicon	–	–	0.06–0.14
Titanium	Balance	Balance	Balance

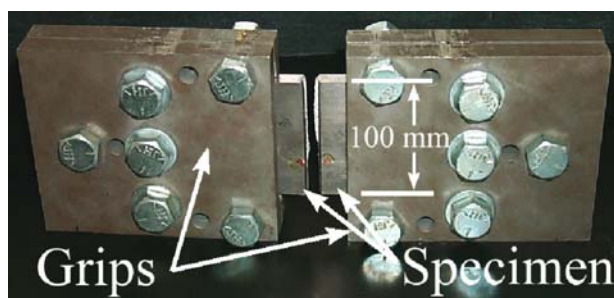
Table 2 Nominal mechanical properties of 6Al-4V Ti, 6Al-4V Ti ELI, and Timetal 5111

Property	6Al-4V Ti	6Al-4V Ti ELI	Timetal 5111
Hardness (Rockwell C)	34	25	28
Ultimate Tensile Strength (MPa)	900	860	850
Yield Strength (MPa)	830	790	745
% Elongation in 2"	10%	10%	13%
% Reduction of Area (Bar)	25%	25%	28.5%
Modulus of Elasticity—Tension (GPa)	114	114	107–114
Modulus of Elasticity—Torsion (GPa)&	42	42	–
Poisson Ratio	0.32	0.32	0.32
Beta Transus (°C)	1000	990	980
Annealing Temperature (°C)	700–830	700–830	–
Forging Temperature (°C)	950	950	–

Experimental Setup

Dynamic tests were performed on three point bend specimens using a lower span of 230 mm except for the ELI titanium. Due to specimen material availability constraints the ELI specimens were held in large steel grips to allow a long 340 mm lower span to be used. Otherwise the lower span would be limited by the specimens' 125 mm length and the specimen would buckle under the impact. The grips are shown holding a broken specimen in Fig. 3. Loading is accomplished by a drop weight tower system. Data is given from tests using 3 m/s and 9 m/s impact speeds.

For the more ductile 6Al-4V Ti ELI and Timetal 5111, the COD technique was used, all on 25% side-grooved specimens save one ungrooved ELI specimen. Strain gages were used with the COD technique to assist in the determination of crack initiation time. The 6Al-4V Ti toughness was measured by all three

**Fig. 3.** Grips used to hold small 6Al-4V Ti ELI specimens for dynamic bend testing**Table 3** Nominal dimensions of three point bend specimens for dynamic fracture toughness testing

Material	a (mm)	W (mm)	B (mm)
6Al-4V Ti	34	100	12.5
6Al-4V Ti ELI	28	93	8–11
Timetal 5111	34	101	15

techniques using both side-grooved and ungrooved specimens. Side-grooves where used were cut by plunge EDM according to ASTM standard *E647-00*. Prior to testing, sharp pre-cracks were produced in all specimens by first cutting a 30 mm notch using wire EDM and then fatiguing 2 mm of crack extension using an MTS system.

Nominal specimen dimensions for the three materials as tested dynamically are given in Table 3. Dimensional variations are due to specimen material availability constraints. With the geometries and setup used, the crack tip loading rate \dot{K} was fairly constant.

Quasistatic tests were also performed on C(T) type specimens as prescribed by ASTM standards [14] *E399-90(1997) Standard Test Method for Plane Strain Fracture Toughness of Metallic Materials*, and *E647-00 Standard Test Method for Measurement of Fatigue Crack Growth Rates* which give the relationship between K_I and applied load and geometry. Table 4 gives specimen nominal dimensions. Some specimens were side-grooved. Again, variation in dimensions was caused by specimen material availability constraints.

Experimental Observations and Results

Initiation Toughness

Initiation toughness versus loading rate for each of the three materials is given in Figs. 4, 5 and 6. Because strain gage data is taken simultaneously with the optical methods and the results agree well for specimens without side-grooves, this data is not included in the plots.

Table 4 Nominal dimensions of C(T) specimens for quasistatic fracture toughness testing

Material	a (mm)	W (mm)	B (mm)
6Al-4V Ti	20–21	84	12.3
6Al-4V Ti ELI	11.4–12.0	77	11.0–12.7
Timetal 5111	17–19	84	15–17

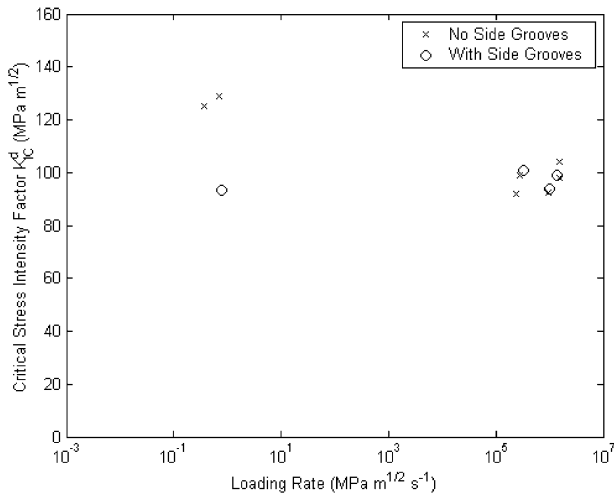


Fig. 4. Initiation toughness versus loading rate for 6Al-4V Ti. (Dynamic values from COD and CGS measurements. See ref [1])

For the 6Al-4V Ti (Fig. 4) under dynamic loading, no significant difference in initiation values were observed between specimens with and without side-grooves, while under quasistatic loading, values for ungrooved specimens are higher (125.1 and 129.1 MPa√m) than that from a specimen with side-grooves (91.3 MPa√m). Assuming that the side-grooved specimen provides a plane strain toughness value, the value from the specimens without side-grooves is about 35% higher. The value of h/r_p for the two specimens without side-grooves is about 5.8, indicating that the thickness effect in this titanium alloy tested quasistatically is more pronounced than in the aluminum tested by Irwin (equation 3, Fig. 1). The toughness for aluminum with the same value of h/r_p is only about 12% above its plane strain toughness.

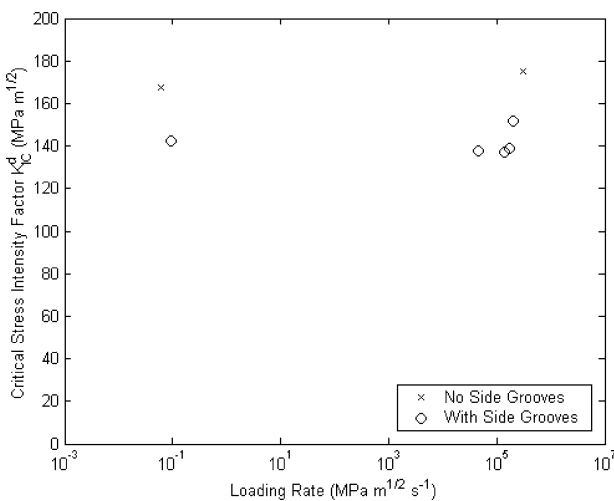


Fig. 5. Initiation toughness versus loading rate for 6Al-4V Ti ELI

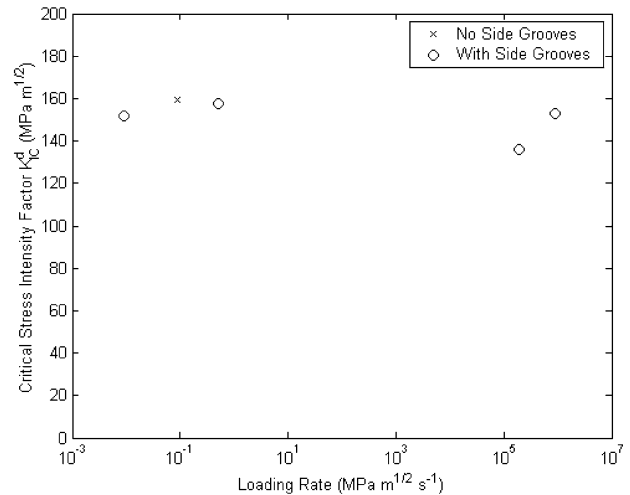


Fig. 6. Initiation toughness versus loading rate for Timetal 5111

Because yield stress increases with strain rate, the characteristic plastic zone size r_p at crack initiation decreases with loading rate (though it increases with K_{IC}^d). Thus for the dynamic specimens the ratio h/r_p is larger, which accounts for the similar initiation values for specimens with and without side-grooves.

In both loading regimes the side-grooved specimens' fracture surfaces have no shear lips as expected. In the ungrooved geometries the quasistatically tested specimen quickly transitions from the shear lip free fatigue crack to 100% shear lips, while the dynamic fracture surfaces transition to less than 25% shear lips. This is consistent with the dynamic fracture being more in a state of plane strain than the quasistatic tests on the same material with same thickness.

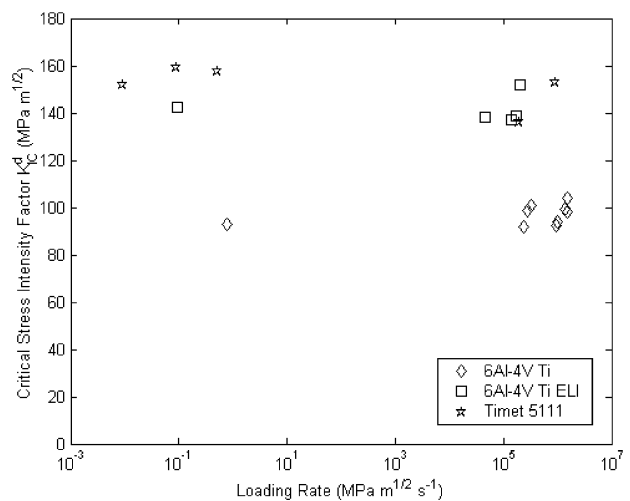


Fig. 7. Plane strain initiation toughness versus loading rate for 6Al-4V Ti, 6Al-4V Ti ELI, and Timetal 5111

For the 6Al-4V Ti ELI (Fig. 5) the ratio h/r_p is about 2.1 for quasistatic loading thus the disparity between initiation toughness values from specimens with and without side-grooves is expected to be significant. In aluminum, quasistatic toughness for the same ratio of h/r_p is 73% higher than its plane strain toughness. With the 6Al-4V Ti ELI for both quasistatic and dynamic regimes the initiation toughness values from specimens without side-grooves is about 20% higher than values from specimens with side-grooves. The increase in h/r_p ratio for dynamic loading is insufficient to reduce the thickness effect, and the fracture surfaces of ungrooved specimens tested quasistatically and dynamically are macroscopically indistinguishable. Thus unlike the 6Al-4V Ti, the 6Al-4V Ti ELI shows a less pronounced thickness effect compared to aluminum.

For the Timetal 5111 (Fig. 6) the ratio h/r_p is about 2.5. Only one specimen without side-grooves was tested, quasistatically. Despite 100% shear lips this specimen provided an initiation toughness in line with those from side-grooved specimens, thus no thickness effect in this material was observed. The grooved specimens have slight curvature in the fracture surface.

For the following comparisons, the results from the side-grooved specimens are assumed to be plane strain values, as well as results from the ungrooved dynamic 6Al-4V Ti tests and the single ungrooved Timetal 5111 quasistatic test. Figure 7 shows these initiation toughnesses versus loading rate for comparison between materials.

Using average plane strain values for the data obtained, the 6Al-4V Ti ELI is 53% tougher than the 6Al-4V Ti under quasistatic conditions and 45% tougher under the dynamic loading conditions of this work. Comparing Timetal 5111 to 6Al-4V Ti, it is 66% and 48% tougher under quasistatic and dynamic loading respectively. Because all three materials have similar elastic properties the differences in toughness must be due to other effects. The fracture surfaces of the 6Al-4V Ti visually appear to have a smooth “satin” finish, while the 5111 surfaces appear very granular and the ELI lies midway in between. In comparing the average of dynamic results with quasistatic values, using plane strain values only, the 6Al-4V Ti dynamic toughness is 4.6% higher than the quasistatic value, with 6Al-4V Ti ELI down 0.7% and Timetal 5111 6.6% lower in toughness. To complete the rate effect picture, more tests should be performed with an effort made to fill in the gap between the quasistatic tests and drop weight dynamic tests, as well as at even higher loading rates. Toughness is reduced by thermal softening and increased by strain rate hardening. At very

high loading rates, the latter effect is expected to dominate and toughness increases. At intermediate rates, two effects are in competition and the toughness may be less than quasistatic values. Such behavior cannot be ruled out for the materials considered here based on the limited data presented.

Using quasistatic initiation toughness values the three materials have characteristic plastic zone sizes (equation 2) as follows: 6Al-4V Ti: 2.2 mm, 6Al-4V Ti ELI: 5.1 mm, Timetal 5111: 6.0 mm.

Conclusions

The application of quasistatic global measurement technique to determine quasistatic stress intensity factors and the optical methods of CGS and COD as well as strain gages to determine dynamic stress intensity factors have been successfully employed to measure the fracture properties of three titanium alloys. The 6Al-4V Ti ELI and Timetal 5111 alloys have significantly higher initiation toughnesses than the commercial grade 6Al-4V Ti alloy. None of the materials showed a significant dependence of plane strain initiation toughness on loading rate at the specific loading rates obtained.

Acknowledgments The authors would like to acknowledge the gracious support of the Office of Naval Research (Steels program and Dr. Julie Christodoulou, program officer, under contract number N00014-01-1-0937. We would also like to extend our gratitude to Prof. G. Ravichandran (Caltech) for his insights shared over numerous conversations.

References

1. Anderson DD, Rosakis AJ (2005) Comparison of three real time techniques for the measurement of dynamic fracture initiation toughness in metals. *Eng Fract Mech* 72:535–555.
2. Ravi-Chandar K, Knauss WG (1984) An experimental investigation into dynamic fracture: I. Crack initiation and arrest. *Int J Fract* 25:247–262.
3. Maigre H, Rittel D (1995) Dynamic fracture detection using the force-displacement reciprocity: Application to the compact compression specimen. *Int J Fract* 73:67–79.
4. Maigre H, Rittel D (1996) A study of mixed-mode dynamic crack initiation in PMMA. *Mech Res Commun* 23:475–481.
5. Maigre H, Rittel D (1996) An investigation of dynamic crack initiation in PMMA. *Mech Mater* 23:229–239.
6. Freund LB, Rosakis AJ (1992) The structure of the near tip-field solution during transient elastodynamic crack growth. *J Mech Phys Solids* 40:699–719.
7. Suresh S, Nakamura T, Yeshurun Y, Yang KH, Duffy J (1990) Tensile fracture-toughness of ceramic material—effects of dynamic loading and elevated-temperatures. *J Am Ceram Soc* 73:2457–2466.

8. Wilson ML, Hawley RH, Duffy J (1980) The effect of loading rate and temperature on fracture initiation in 1020 hot-rolled steel. *Eng Fract Mech* 13:371–385.
9. Dally JW (1979) Dynamic photoelastic studies of fracture. *Exp Mech* 19:349–367.
10. Rosakis AJ, Duffy J, Freund LB (1984) The determination of the dynamic fracture toughness of AISI 4340 steel by the shadow spot method. *J Mech Phys Solids* 34:443–460.
11. Zehnder AT, Rosakis AJ (1990) Dynamic fracture initiation and propagation in 4340 steel under impact loading. *Int J Fract* 43:271–285.
12. Owen DM, Zhuang S, Rosakis AJ, Ravichandran G (1998) Experimental determination of dynamic crack initiation and propagation fracture toughness in thin film aluminum sheets. *Int J Fract* 90:153–174.
13. Irwin GR (1959) Analysis of stresses and strains near the end of a crack traversing a plate. *J Appl Mech* 24:361–364.
14. American Society for Testing and Materials, West Conshohocken, PA 19428-2959, Annual Book of ASTM Standards 2001 Sect. 3 Metals Test Methods and Analytic Procedures; Volume 03.01, Metals—Mechanical Testing; Elevated and Low Temperature Tests; Metallography.
15. Freund LB, Duffy J, Rosakis AJ (1981) Dynamic fracture initiation in metals and preliminary results on the method of caustics for crack propagation measurements. ASME Paper No. 81-PVP-15.
16. Rittel DM, Rosakis AJ (2005) Dynamic fracture of beryllium bulk metallic glass systems: A cross-technique comparison. *Eng Fract Mech* 72:1905–1919.
17. Westergaard HM (1957) On the stress distribution at the base of a stationary crack. *J Appl Mech* 24:109–114.
18. Sneddon IN (1946) Distribution of stress in the neighbourhood of a crack in an elastic solid. *Proc R Soc Lond A* 147:229–260.
19. Williams ML (1939) Bearing pressures and cracks. *J Appl Mech* 6:49–53.
20. Freund LB, Clifton R (1974) On the uniqueness of plane elastodynamic solutions for running cracks. *J Elast* 4:293–299.
21. Yoffe EH (1951) The moving griffith crack. *Phil Mag* 42:739–750.
22. Broberg KB (1960) The propagation of a brittle crack. *Archiv fur Physik* 18:159–192.
23. Atkinson C, Eshelby JD (1968) The flow of energy into the tip of a moving crack. *Int J Fract* 4:3–8.
24. Achenbach JD (1970) Crack propagation generated by a horizontally polarized shear wave. *J Mech Phys Solids* 18:245–259.
25. Achenbach JD (1970) Extension of a crack by a shear wave. *Z Angew Math Phys* 24:887–900.
26. Achenbach JD (1974) Dynamic effects in brittle fracture. In: Nemat-Nasser S (ed) *Mechanics today*. Pergamon, Elmsford, NY, pp 1–57 [chapter 1].
27. Kostrov BV, Nikitin LV (1970) Some general problems of mechanics of brittle fracture. *Arch Mech Stosow* 22:749–775.
28. Freund LB (1972) Crack propagation in an elastic solid subjected to general loading: I. Constant rate of extension. *J Mech Phys Solids* 20:120–140.
29. Freund LB (1972) Crack propagation in an elastic solid subjected to general loading: II. nonuniform rate of extension. *J Mech Phys Solids* 20:141–152.
30. Freund LB (1972) Energy flux into the top of an extending crack in an elastic solid. *J Elast* 2:341–349.
31. Willis JR (1975) Equations of motion for propagating cracks. *The mechanics and physics of fracture*. Metals Soc 0:57–67.
32. Freund LB (1998) *Dynamic fracture mechanics*. Cambridge University Press, New York, NY.
33. Irwin GR (1962) Crack extension force for a part-through crack in a plate. *J Appl Mech* 29:651–654.
34. Kanninen MF, Popelar CH (1985) *Advanced fracture mechanics*. Oxford University Press, New York, NY.
35. Irwin GR (1960) Fracture mode transition for a crack traversing a plate. *J Basic Eng* 82:417–425.
36. Jones MH, Brown Jr WF (1970) The influence of crack length and thickness in plane straining fracture toughness testing. *ASTM STP* 463:63–101.
37. Tippur HV, Krishnaswamy S, Rosakis AJ (1990) A coherent gradient sensor for crack tip deformation measurements: analysis and experimental results. *Int J Fract* 48(1):193–204.
38. Tippur HV, Krishnaswamy S, Rosakis AJ (1991) Optical mapping of crack tip deformations using the methods of transmission and reflection coherent gradient sensing: a study of crack tip K-dominance. *Int J Fract* 52:91–117.
39. Rosakis AJ (1993) Two optical techniques sensitive to gradients of optical path difference: the method of caustics and the coherent gradient sensor {CGS}. In: Epstein JS (ed) *Experimental techniques in fracture*. VCH Publishers. pp 327–425 [chapter 10].
40. Theocaris PS (1981) Elastic stress intensity factors evaluated by caustics. In: Shih GC (ed) *Mechanics of fracture*, vol. VII. Sijthoff and Noordhoff, Roc Alphen aan den Rijn, The Netherlands.
41. Kalthoff JF (1987) Shadow optical methods of caustics. In: Kobayashi AS (ed) *Handbook on experimental mechanics*. McGraw Hill, New York, NY, pp 430–498 [chapter 9].
42. Dally JW, Burger JR (1993) The role of the electric resistance strain gage in fracture research. In: Epstein JS (ed) *Experimental Techniques in Fracture*. VCH Publishers, New York, NY, pp 1–39 [chapter 1].
43. Shih CF (1981) Relationships between the J-integral and the crack opening displacement for stationary and extending cracks. *J Mech Phys Solids* 29(4):305–326.
44. Hutchinson JW (1968) Singular behavior at the end of a tensile crack in a hardening material. *J Mech Phys Solids* 16(13):337.
45. Rice JR, Rosengren GF (1968) Plane strain deformation near a crack tip in a power-law hardening material. *J Mech Phys Solids* 16(1).
46. Costin LS, Duffy J (1979) The effect of loading rate and temperature on the initiation of fracture in a mild, rate sensitive steel. *J Eng Mater Technol* 101:258–264.
47. Nakamura T, Shih CF, Freund LB (1985) Elastic-plastic analysis of a dynamically loaded circumferentially notched round bar. *Eng Fract Mech* 22:437–452.